Editors' Suggestion Featured in Physics

Extensive Spatiotemporal Chaos in Nonreciprocal Flocking

Chul-Ung Woo,[1] Jae Dong Noh,[1,2] and Heiko Rieger[1]

[1]*Department of Theoretical Physics and Center for Biophysics, Saarland University, Saarbrücken, Germany*

[2]*Department of Physics, University of Seoul, Seoul 02504, Korea*

(Received 7 April 2026; accepted 24 June 2026; published 8 September 2026)

Nonreciprocal interactions in active matter give rise to a multitude of fascinating phenomena among which are collective oscillatory states without intrinsic particle chirality and active turbulence. Here we show that, in a paradigmatic model for nonreciprocal flocking, the two-species Vicsek model, these two states coexist: chiral order for small flocks and extensive spatiotemporal chaos for large flocks, both separated by a finite-wavelength instability whose scale is set by the rotation radius of the chiral orbits. For system sizes larger than this length scale extensive spatiotemporal chaos unfolds, as manifested by an extensive number of positive Lyapunov exponents as well as of Floquet exponents, a finite correlation and chaotic length, and a broad energy spectrum. Our results suggest that complex, turbulent behavior is a generic possibility in systems where particles or fields interact asymmetrically and may have significant implications for understanding how nonreciprocal interactions could drive chaotic, fluidlike behavior in active matter.

DOI: 10.1103/lfwy-bbmv

Introduction—Turbulence in passive fluids has long served as a paradigmatic example of collective dynamics in spatially extended nonequilibrium systems [1,2]. In active matter, related phenomena appear as *active turbulence* in bacterial suspensions and active nematics [3–6], where energy is injected at intrinsic small scales rather than transferred through an inertial cascade from the largest scales [5]. From a broader nonlinear-dynamics perspective, turbulence is one manifestation of *extensive spatiotemporal chaos*, which is a dynamical state of an extended system that can be decomposed into many weakly coupled chaotic subsystems, such that the number of positive Lyapunov exponents and the associated Kolmogorov-Sinai entropy scale extensively with system size [7–9]. Classical examples include Rayleigh-Bénard convection [10], reaction-diffusion systems [11], coupled oscillators [12], and complex Ginzburg-Landau dynamics [13]. A common route to such behavior is a *finite-wavelength instability* (FWLI) [2]: sufficiently small systems may sustain a regular pattern or a nearly homogeneous state, whereas beyond a characteristic size the dynamics crosses over to spatiotemporal chaos. The Kuramoto-Sivashinsky equation provides a canonical example of such a system-size-controlled transition [14–16].

Recent work has shown that in active matter [17–20] nonreciprocal interactions, which violate action-reaction symmetry, can generate increasingly complex spatiotemporal dynamics. In scalar active mixtures, it leads to moving and phase-coexisting structures [21] and to chaotic chasing bands in both particle-based and continuum models [22–25]. In flocking mixtures, it likewise gives rise to spatially organized dynamical states, including synchronized bands, chase-and-rest dynamics [26], and species-segregated patterns under exclusive forcing [27] or weak nonreciprocity [28]. More recently, nonreciprocal couplings have also been shown to produce turbulent regimes in active hydrodynamics [29,30]. These studies make clear that nonreciprocity can drive active matter far beyond simple stationary states. Whether nonreciprocal interactions can also invoke extensive spatiotemporal chaos in active matter systems other than hydrodynamic turbulence remains elusive.

To shed light on this question we therefore consider a paradigmatic model for flocking, the Vicsek model, with two nonreciprocally interacting species. For this system, a phase with chiral order was recently predicted [26,31], which is remarkable because it implies the emergence of global rotations of the order parameter in a system of nonchiral particles, in contrast to the chiral systems studied in [3,4,32–38]. As long as density fluctuations are neglected one expects quite generally the periodic motion of a macroscopic order parameter (in flocking systems the angle of the direction of motion) to be described by the Kardar-Parisi-Zhang (KPZ) equation [39–44], indicating the absence of true long-range order. In this Letter we show for the nonreciprocal Vicsek model, which includes density fluctuations, that chiral order survives only below a critical system size set by an FWLI. Beyond this length scale, set by the rotation radius of the chiral orbits, the dynamics exhibits extensive spatiotemporal chaos as we show by analyzing the Boltzmann equation.

Model—We consider a two-species Vicsek-type model with nonreciprocal alignment in two dimensions. Particle i of species $s_i \in \{A, B\}$ has position $\boldsymbol{r}_i$ and heading θ_i and moves at constant speed v_0 in a periodic square of linear size L according to

$$\dot{\boldsymbol{r}}_i = v_0(\cos\theta_i, \sin\theta_i), \tag{1}$$

$$\dot{\theta}_i = \sum_{\alpha\in\{A,B\}} \frac{J_{s_i\alpha}}{N_i^\alpha} \sum_{j\in\mathcal{N}_i^\alpha} \sin(\theta_j - \theta_i) + \sqrt{2T}\xi_i(t), \tag{2}$$

where $\mathcal{N}_i^\alpha$ denotes the neighbors of species α within metric interaction range R around i, $N_i^\alpha = |\mathcal{N}_i^\alpha|$, and the corresponding term is taken to vanish if $N_i^\alpha = 0$. The noise is Gaussian and white, with $\langle\xi_i(t)\xi_j(t')\rangle = \delta_{ij}\delta(t-t')$. Unlike the agent-based dynamics used in Ref. [31], each alignment contribution here is normalized by the instantaneous number of neighbors, N_i^α. Although this normalization can affect quantitative details, it does not alter the main qualitative conclusion; see Supplemental Material (SM) [45].

We set $J_{AA} = J_{BB} = 1$, while nonreciprocity is introduced through unequal interspecies couplings $J_{AB} \neq J_{BA}$. It is convenient to parameterize them by $J_\pm = (J_{AB} \pm J_{BA})/2$, such that $J_- = 0$ is the reciprocal limit and $J_+ = 0$ is the purely antisymmetric line. Unless stated otherwise, we use equal species densities $\rho_A = \rho_B = 3$, interaction range $R = 1$, self-propulsion speed $v_0 = 5$, noise strength $T = 0.1$, and $J_+ = 0$.

Length-scale-dependent instability of the chiral state—In the regime of strong nonreciprocity, $J_- > J_+$, which we consider here, the mean-field theory of Ref. [31] reported a spatially homogeneous time-periodic state and predicted a stable phase with chiral long-range order. We probe the stability of this homogeneous chiral (HC) state using Monte Carlo simulations with an initial condition in which the global polarizations of the two species are offset by $\pi/2$. We find that the stability is strongly system-size dependent [Figs. 1(a)–1(i)]. While the system of size $L = 64$ maintains chiral order throughout the observation time window, chiral order disappears in larger systems: apparently triggered by local defects, the system evolves toward a strongly inhomogeneous state with pronounced species segregation. The decay of chiral order sets in earlier at systems with larger L.

The steady-state phase behavior at large scales is summarized in Fig. 1(m). Along the cut $J_- = 0.7$, the system

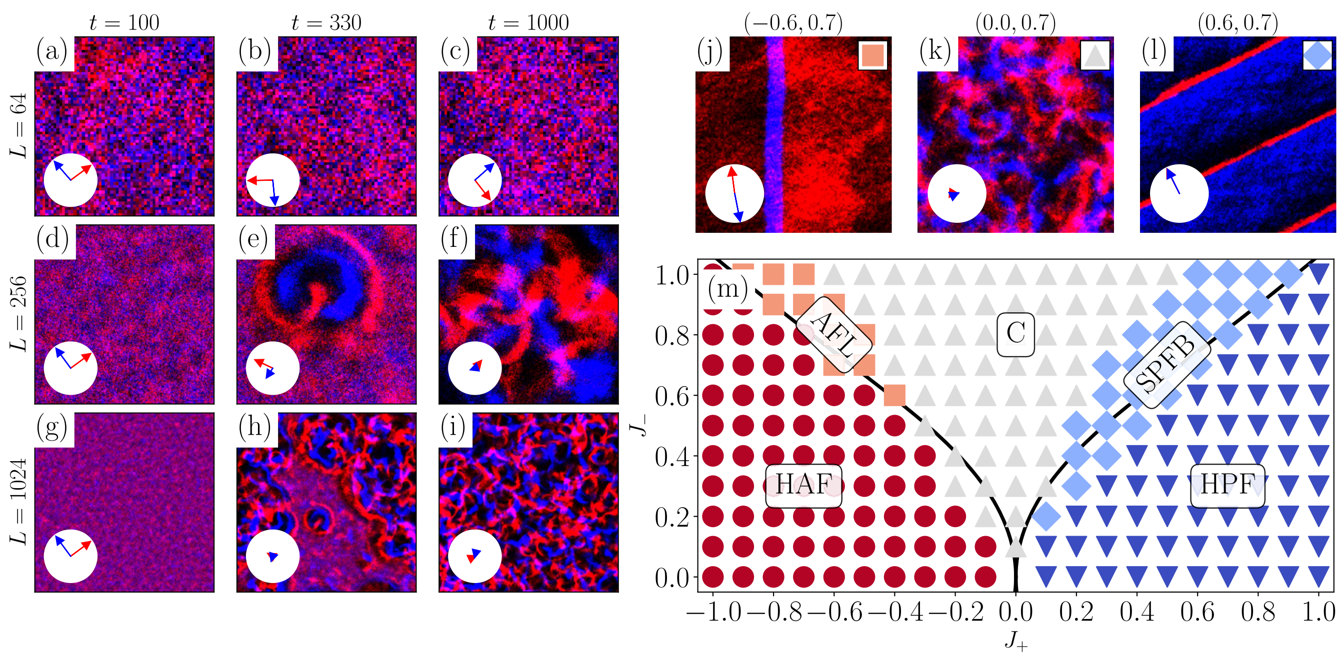

FIG. 1. Microscopic dynamics and phase behavior of the two-species nonreciprocal Vicsek model. Species A is shown in red, and species B is in blue. (a)–(i) Snapshots at $J_- = 0.3$ for $L = 64$, 256, 1024 (top to bottom) at $t = 100$, 330, 1000 (left to right). White insets: the instantaneous global polarizations of the two species. (j)–(l) Representative steady-state snapshots at $J_- = 0.7$, $J_+ = -0.6$, 0, 0.6, and $L = 256$. (m) Microscopic phase diagram in the (J_+, J_-) plane. Circles denote homogeneous antiparallel flocking (HAF), squares are a longitudinal antiparallel flocking lane (AFL), upward triangles are the chaotic phase (C), diamonds are a species-separated parallel flocking band (SPFB), and downward triangles are homogeneous parallel flocking (HPF). The black line indicates the exceptional transition predicted by the mean-field theory of Ref. [31].

passes through a sequence of distinct states as $|J_+|$ is reduced: for large negative and positive J_+, it remains in the trivial homogeneous antiparallel and parallel flocking states, respectively, while at intermediate values it develops a longitudinal antiparallel flocking lane [Fig. 1(j)] for $J_+ < 0$ and a species-separated parallel flocking band [Fig. 1(l)] for $J_+ > 0$. Near $J_+ = 0$, these ordered structures give way to a chaotic phase [Fig. 1(k)]. The black line in Fig. 1(m) indicates the exceptional transition predicted by the mean-field theory of Ref. [31]. The main qualitative deviation from the phase diagram in [31] occurs near the antisymmetric line $J_+ = 0$, where the mean-field HC state claimed in [31] is replaced by the chaotic phase. In the following, we show that the decay of chiral order is controlled by an FWLI.

Global chirality and decay time—We define the global chirality χ as the particle-averaged deterministic part of the angular velocity, i.e., the right side of Eq. (2) without the noise term. Thus, χ measures the net collective rotation and vanishes in the absence of collective chiral motion. As shown in Fig. 2(a), $\chi(t)$ remains finite in small systems, indicating a stable HC state over the observation window. By contrast, in larger systems $\chi(t)$ decays to zero in a characteristic decay time, signaling the destabilization of the HC state.

To analyze the mechanism leading to the destruction of the chiral state we determine its decay time τ_d. We define τ_d as the onset time of the localized species-segregated breakdown visible in Fig. 1(e), using a criterion specified in SM [45]. Figure 2(b) shows the survival probability $\mathrm{Prob}(\tau_d > t)$ for several system sizes at fixed $J_- = 0.2$. The survival probability converges to a finite value for $L = 64$, indicating apparent long-lived stability of the chiral state, but decays to zero for larger values of L. The survival probability curve suggests convergence to a step function sitting at finite τ_∞. This behavior is incompatible with a picture of instability due to spatially independent Poisson nucleation events of defects, which in two dimensions would instead imply a characteristic decay time scaling as L^{-2}. This differentiates the present mechanism from that reported in the active Ising model where an ordered phase is metastable due to spontaneously nucleated droplets [51,52]. The present mechanism is more consistent with an FWLI, which we confirm below.

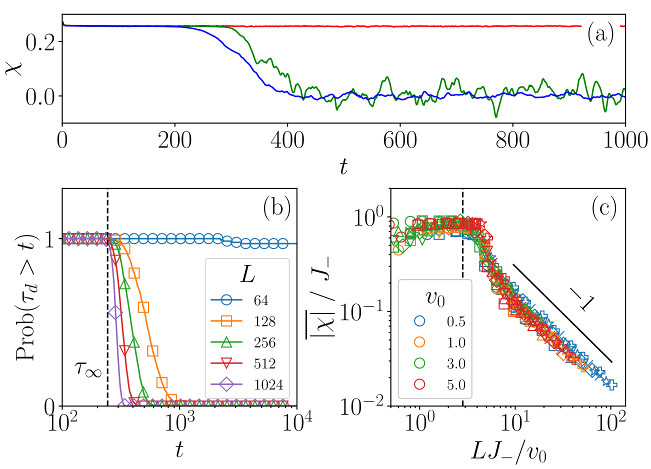

FIG. 2. (a) Time evolution of the global chirality $\chi(t)$ of Figs. 1(a)–1(i); the three curves correspond to $L = 64$ (red), 256 (green), and 1024 (blue). (b) Survival probability $\mathrm{Prob}(\tau_d > t)$ at $J_- = 0.2$, where τ_d denotes the onset time of the local breakdown of the prepared HC state; the dashed line marks the decay time τ_∞ in the infinite size limit. (c) Finite-size data collapse analysis of the scaled time-averaged chirality $\overline{|\chi|}/J_-$ against a scaling variable LJ_-/v_0 for different self-propulsion speeds v_0. The vertical dashed line indicates the geometric crossover estimate, $2\sqrt{2}$. Different marker shapes indicate different values of J_-; the full marker legend is provided in SM [45].

The long-time-averaged chirality obeys a simple finite-size scaling form. Since the microscopic rotation rate is proportional to J_-, it is natural to write $\chi(J_-; L, v_0) = J_- \chi_r(x)$ with $x = LJ_-/v_0 \sim L/r_{\mathrm{rot}}$, where $r_{\mathrm{rot}} \sim v_0/J_-$ is the rotation radius of a chiral orbit. Figure 2(c) shows that the data collapse well when $\overline{|\chi|}/J_-$ is plotted against the scaling variable LJ_-/v_0. The vertical dashed line indicates a crossover scale, which is estimated geometrically using an ideal circular orbit [45]. The crossover scale estimated in this way will be called a geometric crossover estimate.

For small x, $\chi_r(x)$ is approximately constant, corresponding to the regime in which the HC state remains stable. For large x, the data decay approximately as x^{-1}, indicating that the global chirality vanishes in the thermodynamic limit. This collapse identifies r_{rot} as the intrinsic length scale controlling the finite-size crossover. When L is not larger than this rotation-controlled scale, each particle of one species explores a substantial fraction of the orbit of the other species, so the interspecies coupling becomes mean-field-like. As we show below, the wavelength selected by the kinetic instability is tied to this same intrinsic scale.

Boltzmann kinetic description—To connect the microscopic dynamics to a continuum description, we introduce for each species $\alpha \in \{A, B\}$ a one-particle distribution $f^\alpha(\boldsymbol{r}, \theta, t)$. Under the assumptions of dilute binary collisions and molecular chaos, in the spirit of standard Boltzmann descriptions of aligning active particles [53,54], it obeys

$$\partial_t f^\alpha + v_0 \hat{\boldsymbol{e}}(\theta) \cdot \nabla f^\alpha = I_{\mathrm{sd}}[f^\alpha] + \sum_{\beta \in \{A,B\}} I_{\mathrm{coll}}[f^\alpha, f^\beta]. \qquad (3)$$

Here, $\hat{\boldsymbol{e}}(\theta) = (\cos\theta, \sin\theta)$, I_{sd} describes angular self-diffusion, and I_{coll} is binary interactions.

After nondimensionalizing space and time, we expand $f^\alpha(\boldsymbol{r}, \theta, t)$ in angular Fourier modes $f_k^\alpha(\boldsymbol{r}, t)$. The zeroth and first modes, f_0^α and f_1^α, are proportional to the density and the complex polarization field, respectively. The resulting mode hierarchy reads as

$$\partial_t f_k^\alpha + \left(\partial_{z^*} f_{k-1}^\alpha + \partial_z f_{k+1}^\alpha\right) = -(1-P_k) f_k^\alpha + \sum_\beta \sum_{l=-\infty}^{\infty} \kappa^{\alpha\beta} J_{k,l}^{\alpha\beta} f_{k-l}^\alpha f_l^\beta, \quad (4)$$

where $z = x + iy$, $\partial_z = (\partial_x - i\partial_y)/2$, and $\partial_{z^*} = (\partial_x + i\partial_y)/2$. Here P_k is the kth Fourier coefficient of the self-diffusion kernel, $J_{k,l}^{\alpha\beta}$ encodes the nature of the interactions (aligning or antialigning), and the coefficients $\kappa^{\alpha\beta}$ set the interaction strength; see SM [45]. Throughout this Letter, we fix $\kappa^{AA} = \kappa^{BB} = 0.5$ and vary $\kappa^{AB} = \kappa^{BA} = \kappa$. With this choice, the model corresponds to the microscopic model with $J_+ = 0$ and $J_- > 0$. To obtain a closed kinetic description, we truncate the angular Fourier hierarchy at $k = 4$.

Floquet stability analysis—We found that the Boltzmann equation limited to a homogeneous manifold allows for a HC solution in which the polarizations perform limit cycle motion of period $\mathcal{T}$ and chirality $\chi = 2\pi/\mathcal{T}$. We perform a quantitative analysis of the stability of this state against a position-dependent random perturbation using the Floquet method [55].

It is convenient to work in the spatial Fourier space labeled by a wave vector $\boldsymbol{q}$. Taking the HC solution, computed numerically, as a reference state, we initialize random perturbations for all Fourier modes with nonzero $\boldsymbol{q}$. This perturbed state is evolved over one period $\mathcal{T}$, the growth rate of each mode at $\boldsymbol{q}$ is measured, and the amplitudes of perturbed modes are rescaled back to their initial values. Repeating this procedure iteratively, we can obtain a local Floquet exponent $\Lambda(\boldsymbol{q})$.

Figure 3(a) shows $\Lambda(q)$, radially averaged $\Lambda(\boldsymbol{q})$ over all $\boldsymbol{q}$ with given $q = |\boldsymbol{q}|$, for several values of η at fixed $\kappa = 0.1$. In all cases considered, the dominant peak lies at finite q, showing that the HC motion is destabilized by a finite-wavelength mode. The corresponding wavelength $\ell_m = 2\pi/q_m$, determined by the wave number q_m of the maximally unstable mode, is shown in Fig. 3(b) through the rescaled quantity $\chi\ell_m$. In the weak-coupling regime, $\chi\ell_m$ remains approximately constant. This behavior is on par with the crossover in the microscopic model occurring at $L \sim r_{\mathrm{rot}}$. We note that the plateau value of χl_m is close to the geometric crossover estimate indicated by the horizontal dashed line. Therefore we conclude that the FWLI of the Boltzmann equation is related to the finite-size destabilization of the HC state in the particle model. Deviations from this weak-coupling correspondence at larger κ and η are discussed in SM [45].

Figure 3(c) shows the number of unstable modes N_+, defined as the number of Fourier modes with a positive Floquet exponent. This number grows linearly with the system area, $N_+ \sim L^2$, meaning that it is extensive.

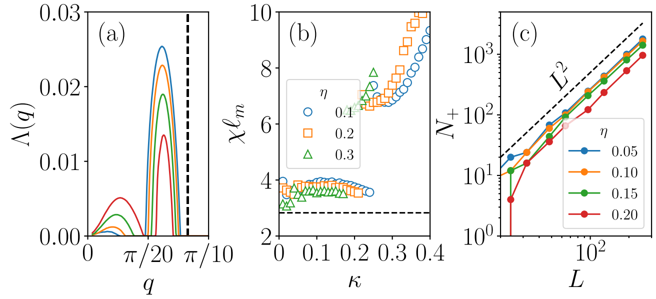

FIG. 3. (a) Floquet exponents $\Lambda(q)$ as functions of wave number q at several values of η at $\kappa = 0.1$. The colors are the same as in panel (c). (b) Rescaled wavelength $\chi\ell_m$ of the most unstable mode as a function of κ for several values of η. (c) Number of positive Floquet exponents, N_+, as a function of system size L. The dashed line is a guide to the eye proportional to L^2.

Evidence for extensive spatiotemporal chaos (ESTC)—We proceed further beyond the linear Floquet stability analysis by calculating the Lyapunov exponents characterizing the exponential rate of separation of infinitesimally close trajectories in the steady state (see SM [45] for the numerical method). Figure 4(a) shows the Lyapunov exponents λ_m, sorted in descending order, in the chaotic regime. The largest Lyapunov exponent is positive. Moreover, the number of positive Lyapunov exponents N_+^{Lya} scales extensively with the system size as L^2, which is a hallmark of ESTC [8,9]. In SM [45], we show that the Kolmogorov-Sinai entropy is also extensive, the velocity-velocity correlations are short ranged, and the energy spectrum is broad, which all point toward ESTC.

Complementary evidence for ESTC comes from the observation that the chaotic state can be decomposed into weakly coupled chaotic areas of the size of the instability length scale that we identified above. For this purpose we implemented a master-slave protocol as described in the context of synchronization of chaotic PDEs and turbulence [56–58]. As in the setup for the Lyapunov exponent, we prepare unperturbed and perturbed states, which are referred to as master and slave states, respectively. We introduce a circular region (*free core*) of radius r_{core} [see Fig. 4(b)] and impose an additional unidirectional coupling: the slave state evolves independently of the master state inside the free core but is attracted toward the master state outside the free core. If r_{core} is smaller than the chaotic length scale, the slave state within the free core gets enslaved by the field outside the free core, i.e., the master state. Otherwise, the slave state develops its own chaotic evolution. Figures 4(d) and 4(e) illustrate these two cases for a small and a large r_{core}, respectively. This behavior is quantified by a mismatch $E_{\mathrm{core}}(t)$, defined as a relative deviation between the master and slave states within the free core (see SM [45]), shown in Fig. 4(f): for small cores the mismatch decays to zero, whereas for

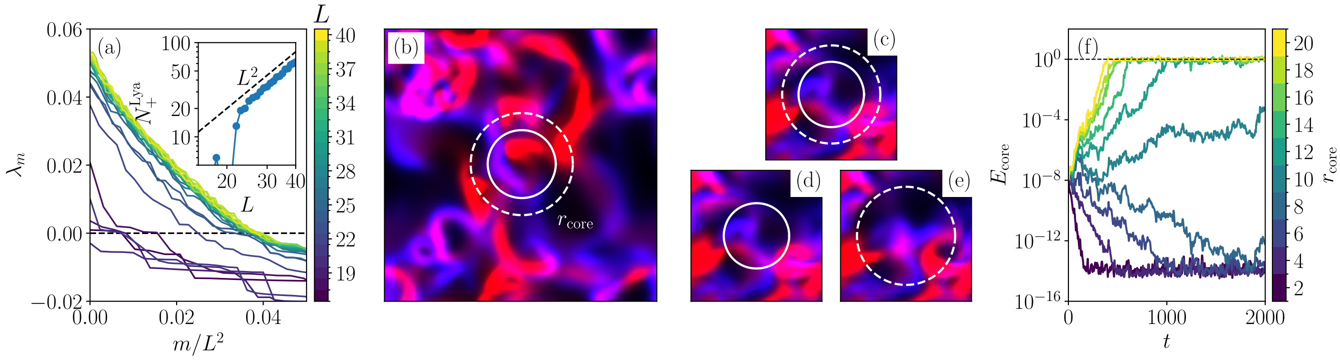

FIG. 4. (a) Lyapunov spectrum λ_m plotted against the rescaled index m/L^2. Inset: $N_+^{\rm Lya}$, the number of positive Lyapunov exponents, scales as L^2. (b) A snapshot of a chaotic master state; the solid and dashed circles indicate two representative free core radii $r_{\rm core}$. (c) Enlarged view of the master state in (b) after some time. (d),(e) Snapshots of slave states associated with the free cores with $r_{\rm core} = 8$ and 12, respectively. (f) Mismatch $E_{\rm core}$ versus time for different $r_{\rm core}$. Slave states with small cores synchronize to the master state, whereas with large cores they evolve independently, revealing a finite chaotic length scale. Parameters: $\kappa = 0.2, \eta = 0.1$. (b)–(f) $L = 64$.

sufficiently large cores it remains finite at long times. The crossover occurring at $r_{\rm core} \sim 10$ identifies a finite chaotic length scale, beyond which different regions behave as independent chaotic subsystems. The corresponding diameter agrees with the system size $L \simeq 22$ above which $N_+^{\rm Lya}$ exhibits extensive scaling. Together with the diagnostics above, this consistency indicates that the large-scale kinetic state exhibits ESTC.

Discussion—We have shown that the homogeneous chiral state of the nonreciprocal Vicsek model is not the asymptotic large-scale state in two dimensions [59]. Instead, it exists only below a characteristic scale set by the radius of the chiral orbit and is destabilized at larger scales due to a finite-wavelength instability. This size-dependence has to be distinguished from finite-size effects at conventional phase transitions which just smooth the critical singularity [62] and from a crossover from chiral order to KPZ behavior in chiral Malthusian flocks [44]. One reason that a KPZ behavior for periodic motion of a macroscopic order parameter [39–44] is not observable in the nonreciprocal Vicsek model might be the relevance of density fluctuations: in Figs. 1(e) and 1(h), as well as in Movies 2 and 3 in SM [45], one sees that within the chiral ordered state first localized droplets of species-segregated density fluctuation emerge and then they expand and destroy chiral order. The FWLI is also different from metastability due to nucleation of local defects [51,52]. The system size acts here like a parameter triggering the transition from an ordered to a chaotic state, like frequently in turbulence and specifically in the Kuramoto-Sivashinsky equation [2,14].

In the nonreciprocal Vicsek model the transition is accompanied by the loss of global chirality and the emergence of extensive spatiotemporal chaos. In connection with recent works on nonreciprocal turbulence, notably in binary-fluid systems [29,30], our results suggest that complex, turbulent behavior is a generic possibility in systems where particles or fields interact asymmetrically. This may have significant implications for understanding how nonreciprocal interactions could drive chaotic, fluid-like behavior in active matter. It also provides a new mechanism for turbulence that does not require traditional geometric or external triggers.

Note added—We became aware of a study of the discrete nonreciprocal Vicsek model reporting the destruction of chiral order by the nucleation of defects, as given in the following Letter [63].

Acknowledgments—This work was supported by the National Research Foundation of Korea (NRF) grant funded by the Korea government (MSIT) under Grant No. RS-2024-00348526 and in part by Grant No. NSF PHY-2309135 to the Kavli Institute for Theoretical Physics (KITP). We acknowledge the Urban Big Data and AI Institute of the University of Seoul supercomputing resources made available for conducting the research reported in this paper.

Data availability—There are no publicly available research data or software supporting this manuscript. Requests for further information or data should be sent to the authors.

[1] U. Frisch, *Turbulence: The Legacy of A. N. Kolmogorov* (Cambridge University Press, Cambridge, England, 2010).
[2] M. C. Cross and P. C. Hohenberg, Pattern formation outside of equilibrium, Rev. Mod. Phys. **65**, 851 (1993).
[3] H. H. Wensink, J. Dunkel, S. Heidenreich, K. Drescher, R. E. Goldstein, H. Löwen, and J. M. Yeomans, Meso-scale turbulence in living fluids, Proc. Natl. Acad. Sci. U.S.A. **109**, 14308 (2012).

[4] J. Dunkel, S. Heidenreich, K. Drescher, H. H. Wensink, M. Bär, and R. E. Goldstein, Fluid dynamics of bacterial turbulence, Phys. Rev. Lett. **110**, 228102 (2013).
[5] R. Alert, J. Casademunt, and J.-F. Joanny, Active turbulence, Annu. Rev. Condens. Matter Phys. **13**, 143 (2022).
[6] V. Bratanov, F. Jenko, and E. Frey, New class of turbulence in active fluids, Proc. Natl. Acad. Sci. U.S.A. **112**, 15048 (2015).
[7] D. Ruelle, Large volume limit of the distribution of characteristic exponents in turbulence, Commun. Math. Phys. **87**, 287 (1982).
[8] H.-W. Xi, R. Toral, J. D. Gunton, and M. I. Tribelsky, Extensive chaos in the Nikolaevskii model, Phys. Rev. E **62**, R17 (2000).
[9] S. Tajima and H. S. Greenside, Microextensive chaos of a spatially extended system, Phys. Rev. E **66**, 017205 (2002).
[10] D. A. Egolf, I. V. Melnikov, W. Pesch, and R. E. Ecke, Mechanisms of extensive spatiotemporal chaos in Rayleigh–Bénard convection, Nature (London) **404**, 733 (2000).
[11] Y. Kuramoto, Diffusion-induced chaos in reaction systems, Prog. Theor. Phys. Suppl. **64**, 346 (1978).
[12] G. Hu, Y. Zhang, H. A. Cerdeira, and S. Chen, From low-dimensional synchronous chaos to high-dimensional desynchronous spatiotemporal chaos in coupled systems, Phys. Rev. Lett. **85**, 3377 (2000).
[13] I. S. Aranson and L. Kramer, The world of the complex Ginzburg–Landau equation, Rev. Mod. Phys. **74**, 99 (2002).
[14] Y. Kuramoto, *Chemical Oscillations, Waves, and Turbulence* (Springer, New York, 1984).
[15] D. T. Papageorgiou and Y. S. Smyrlis, The route to chaos for the Kuramoto–Sivashinsky equation, Theor. Comput. Fluid Dyn. **3**, 15 (1991).
[16] R. W. Wittenberg and P. Holmes, Scale and space localization in the Kuramoto–Sivashinsky equation, Chaos **9**, 452 (1999).
[17] M. C. Marchetti, J.-F. Joanny, S. Ramaswamy, T. B. Liverpool, J. Prost, M. Rao, and R. A. Simha, Hydrodynamics of soft active matter, Rev. Mod. Phys. **85**, 1143 (2013).
[18] C. Bechinger, R. Di Leonardo, H. Löwen, C. Reichhardt, G. Volpe, and G. Volpe, Active particles in complex and crowded environments, Rev. Mod. Phys. **88**, 045006 (2016).
[19] M. R. Shaebani, A. Wysocki, R. G. Winkler, G. Gompper, and H. Rieger, Computational models for active matter, Nat. Rev. Phys. **2**, 181 (2020).
[20] M. te Vrugt and R. Wittkowski, Metareview: A survey of active matter reviews, Eur. Phys. J. E **48**, 12 (2025).
[21] A. Dinelli, J. O'Byrne, A. Curatolo, Y. Zhao, P. Sollich, and J. Tailleur, Non-reciprocity across scales in active mixtures, Nat. Commun. **14**, 7035 (2023).
[22] Y. Duan, J. Agudo-Canalejo, R. Golestanian, and B. Mahault, Dynamical pattern formation without self-attraction in quorum-sensing active matter: The interplay between nonreciprocity and motility, Phys. Rev. Lett. **131**, 148301 (2023).
[23] Y. Duan, J. Agudo-Canalejo, R. Golestanian, and B. Mahault, Phase coexistence in nonreciprocal quorum-sensing active matter, Phys. Rev. Res. **7**, 013234 (2025).
[24] F. Brauns and M. C. Marchetti, Nonreciprocal pattern formation of conserved fields, Phys. Rev. X **14**, 021014 (2024).
[25] S. Saha and R. Golestanian, Effervescence in a binary mixture with nonlinear non-reciprocal interactions, Nat. Commun. **16**, 7310 (2025).
[26] D. Martin, D. Seara, Y. Avni, M. Fruchart, and V. Vitelli, Transition to collective motion in nonreciprocal active matter: Coarse graining agent-based models into fluctuating hydrodynamics, Phys. Rev. X **15**, 041015 (2025).
[27] K. L. Kreienkamp and Sabine H. Klapp, Nonreciprocal alignment induces asymmetric clustering in active mixtures, Phys. Rev. Lett. **133**, 258303 (2024).
[28] C. Myin and B. Mahault, Flocking in weakly nonreciprocal mixtures, arXiv:2510.25377.
[29] J. U. Klamser and L. Berthier, Directed percolation transition to active turbulence driven by non-reciprocal forces, arXiv:2510.04575.
[30] B. Maji, N. B. Padhan, and R. Pandit, Non-reciprocal binary-fluid turbulence, arXiv:2602.06928.
[31] M. Fruchart, R. Hanai, P. B. Littlewood, and V. Vitelli, Non-reciprocal phase transitions, Nature (London) **592**, 363 (2021).
[32] B. Liebchen and D. Levis, Chiral active matter, Europhys. Lett. **139**, 67001 (2022).
[33] J. Mecke, J. O. Nketsiah, R. Li, and Y. Gao, Emergent phenomena in chiral active matter, Natl. Sci. Open **3**, 20230086 (2024).
[34] Y. Sumino, K. H. Nagai, Y. Shitaka, D. Tanaka, K. Yoshikawa, H. Chaté, and K. Oiwa, Large-scale vortex lattice emerging from collectively moving microtubules, Nature (London) **483**, 448 (2012).
[35] L. Giomi, M. J. Bowick, X. Ma, and M. C. Marchetti, Defect annihilation and proliferation in active nematics, Phys. Rev. Lett. **110**, 228101 (2013).
[36] K. Han, G. Kokot, O. Tovkach, A. Glatz, I. S. Aranson, and A. Snezhko, Emergence of self-organized multivortex states in flocks of active rollers, Proc. Natl. Acad. Sci. U.S.A. **117**, 9706 (2020).
[37] H. Wioland, F. G. Woodhouse, J. Dunkel, J. O. Kessler, and R. E. Goldstein, Confinement stabilizes a bacterial suspension into a spiral vortex, Phys. Rev. Lett. **110**, 268102 (2013).
[38] E. Lushi, H. Wioland, and R. E. Goldstein, Fluid flows created by swimming bacteria drive self-organization in confined suspensions, Proc. Natl. Acad. Sci. U.S.A. **111**, 9733 (2014).
[39] M. Kardar, G. Parisi, and Y.-C. Zhang, Dynamic scaling of growing interfaces, Phys. Rev. Lett. **56**, 889 (1986).
[40] G. Grinstein, D. Mukamel, R. Seidin, and C. H. Bennett, Temporally periodic phases and kinetic roughening, Phys. Rev. Lett. **70**, 3607 (1993).
[41] H. Chaté, G. Grinstein, and L.-H. Tang, Long-range correlations in systems with coherent (quasi)periodic oscillations, Phys. Rev. Lett. **74**, 912 (1995).
[42] R. Daviet, C. P. Zelle, A. Asadollahi, and S. Diehl, Kardar-Parisi-Zhang scaling in time-crystalline matter, Phys. Rev. Lett. **135**, 047101 (2025).
[43] A. Maitra, Activity unmasks chirality in liquid-crystalline matter, Annu. Rev. Condens. Matter Phys. **16**, 275 (2025).
[44] L. Chen, C. F. Lee, and J. Toner, Only the ambidextrous can flock: Two-dimensional chiral Malthusian flocks, time

cholesterics, and the Kardar-Parisi-Zhang equation, Phys. Rev. E **113**, 045419 (2026).

[45] See Supplemental Material at http://link.aps.org/supplemental/10.1103/lfwy-bbmv for details on the model and numerical analyses, which includes Refs. [45–50].

[46] A. N. Kolmogorov, A refinement of previous hypotheses concerning the local structure of turbulence in a viscous incompressible fluid at high Reynolds number, J. Fluid Mech. **13**, 82 (1962).

[47] I. Shimada and T. Nagashima, A numerical approach to ergodic problem of dissipative dynamical systems, Prog. Theor. Phys. **61**, 1605 (1979).

[48] G. Benettin, L. Galgani, A. Giorgilli, and J.-M. Strelcyn, Lyapunov characteristic exponents for smooth dynamical systems and for Hamiltonian systems; A method for computing all of them. Part 1: Theory, Meccanica **15**, 9 (1980).

[49] J.-P. Eckmann and D. Ruelle, Ergodic theory of chaos and strange attractors, Rev. Mod. Phys. **57**, 617 (1985).

[50] B. Mahault, Outstanding problems in the statistical physics of active matter, Ph.D. thesis, Université Paris Saclay (COmUE), 2018.

[51] B. Benvegnen, O. Granek, S. Ro, R. Yaacoby, H. Chaté, Y. Kafri, D. Mukamel, A. Solon, and J. Tailleur, Metastability of discrete-symmetry flocks, Phys. Rev. Lett. **131**, 218301 (2023).

[52] C.-U. Woo and J. D. Noh, Motility-induced pinning in flocking system with discrete symmetry, Phys. Rev. Lett. **133**, 188301 (2024).

[53] E. Bertin, M. Droz, and G. Grégoire, Boltzmann and hydrodynamic description for self-propelled particles, Phys. Rev. E **74**, 022101 (2006).

[54] E. Bertin, M. Droz, and G. Grégoire, Hydrodynamic equations for self-propelled particles: Microscopic derivation and stability analysis, J. Phys. A **42**, 445001 (2009).

[55] D. Barkley and R. D. Henderson, Three-dimensional Floquet stability analysis of the wake of a circular cylinder, J. Fluid Mech. **322**, 215 (1996).

[56] L. Kocarev, Z. Tasev, and U. Parlitz, Synchronizing spatiotemporal chaos of partial differential equations, Phys. Rev. Lett. **79**, 51 (1997).

[57] C. C. Lalescu, C. Meneveau, and G. L. Eyink, Synchronization of chaos in fully developed turbulence, Phys. Rev. Lett. **110**, 084102 (2013).

[58] A. Karimi and M. R. Paul, Length scale of a chaotic element in Rayleigh-Bénard convection, Phys. Rev. E **86**, 066212 (2012).

[59] Notably, nonreciprocity due to small symmetric phase shifts in the alignment interactions between multiple species does exhibit quasi-long-range chiral order [60,61].

[60] C.-U. Woo, H. Rieger, and J. D. Noh, Collective behavior in the nonreciprocal multi-species Vicsek model, arXiv:2512.18756.

[61] C.-U. Woo, H. Rieger, and J. D. Noh, Nonreciprocal yet symmetric multi-species active matter: Emergence of chirality and species separation, arXiv:2512.18749.

[62] K. Binder, Finite size effects on phase transitions, Ferroelectrics **73**, 43 (1987).

[63] C. Myin, S. Saha, and B. Mahault, following Letter, Breakdown of emergent chiral order and defect chaos in nonreciprocal flocks, Phys. Rev. Lett. **137**, 118302 (2026).